Magnetic resonance imaging of alginate beads containing pancreatic beta cells and paramagnetic nanoparticles

This article was published in ACS Biomaterials Science and Engineering:

https://doi.org/10.1021/acsbiomaterials.7b00404

AUTHOR NAMES

Sary Sarkis[1,‡], Fanny Silencieux [2, 3, 4,‡], Karen E. Markwick [1], Marc-André Fortin [2, 3, 4,], Corinne A. Hoesli [1,*]*

AFFILIATIONS

1. Department of Chemical Engineering, Wong Building, 3610 University Street, Montreal, QC, H3A 0C5, Canada.
2. Laboratoire de Biomatériaux pour l'Imagerie médicale, Axe Médecine Régénératrice, Centre de recherche du Centre hospitalier universitaire de Québec (CR-CHUQ), 10 rue de l'Espinay, Québec, QC G1L 3L5, Canada.
3. Centre de recherche sur les matériaux avancés (CERMA), Pavillon Vachon, 1065 avenue de la Médecine, Université Laval, Quebec City (QC), G1V 0A6, Canada
4. Département de Génie des Mines, de la Métallurgie et des Matériaux, Pavillon Pouliot, 1065 avenue de la Médecine, Université Laval, Quebec City (QC), G1V 0A6, Canada

*Corresponding authors. E-mail: corinne.hoesli@mcgill.ca; marc-andre.fortin@gmn.ulaval.ca

‡These authors contributed equally.

ABSTRACT

Microencapsulation is being investigated as a means to avoid rejection of transplanted pancreatic islets. Monitoring bead distribution and stability in vivo is an important step towards improving microencapsulated islet transplantation strategies. Islet co-encapsulation with gadolinium-labeled mesoporous silica nanoparticles (Gd-MSNs) could provide a means to visualise the beads while immobilizing and limiting the potential internalisation of the contrast agent. The porous nature of the MSNs could also be used to locally release anti inflammatory, angiogenic, or anti apoptotic factors. Mouse insulinoma 6 (MIN6) beta cells were co-encapsulated with Gd-MSNs in alginate beads produced by emulsification and internal gelation. Gd-MSN alginate beads appeared brighter in T_1-w. imaging sequences (detection threshold of 0.016 mM Gd; relaxometric ratio $r_2/r_1 = 1.45$). No leaching of Gd^{3+} from the hydrogels was detected over the course of 3 months. Cells co-encapsulated with Gd-MSNs were viable without significant differences in cell growth rate compared to controls. This study paves the way towards microencapsulated islet tracking via MRI using co-encapsulated paramagnetic nanomaterials.

KEYWORDS

Islet encapsulation, magnetic resonance imaging, alginate beads, beta cell, paramagnetic contrast agents, mesoporous silica nanoparticles

INTRODUCTION

Type 1 diabetes is a chronic disease caused by the autoimmune destruction of insulin-producing pancreatic beta cells. The economic burden of this disease is estimated to represent ~14.5 billion dollars annually in the United States[1] and 1.4 billion in Canada.[2] Over the last decades, islet transplantation has emerged as a promising alternative to traditional insulin therapy. In this procedure, human islets are procured from the pancreas of irreversibly comatose donors, and introduced into the hepatic portal vein of the patient. Data from the Collaborative Islet Transplant Registry indicates that 44% of islet transplant recipients treated between 2007-2010 achieved insulin independence for at least 3 years.[3] Even in patients that did not achieve long-term insulin independence, islet transplantation significantly reduced severe hypoglycemic episodes and hemoglobin A1c levels for at least 1 year.[4-5] Due to the limited donor islet supply and the current need for lifelong immunosuppression following islet transplantation, this therapeutic option remains inaccessible to the majority of patients. Even with improvements in islet isolation methods and immunosuppressive regimens, the majority of islet transplant recipients revert to insulin dependence after 3 to 5 years.[6] The immunosuppressive regimen used to avoid islet rejection may contribute to the progressive loss of graft function.[7-8]

For over 3 decades, islet microencapsulation has been studied as a method to protect transplanted cells from the host immune system.[9] Islet encapsulation could reduce or even eliminate the need for chronic immunosuppression, increasing graft longevity and patient accessibility to the treatment. Long-term blood glucose normalization has been achieved in animal models of autoimmune diabetes.[10-12] However, reproducing these promising results in primates including humans has been challenging.[13]

The most common microencapsulated islet transplantation site is the peritoneal cavity due to the significant increase in graft volume compared to non-encapsulated islets.[14] However, the lack of control over bead localization within the peritoneal cavity may lead to variable levels of bead fibrotic overgrowth, bead movement and bead agglomeration, all of which may exacerbate the oxygen mass transfer limitations that lead to islet dysfunction and hypoxic cell death. This could also explain the ~5 to 10-fold higher islet doses required to achieve blood glucose normalization using encapsulated islets compared to non-encapsulated syngeneic islets in rodents[15]. Nutrient mass transfer limitations due to bead sedimentation and agglomeration may be even more problematic in larger animals, particularly bipeds.[16]

To correlate the viability and function of encapsulated islets with the graft anatomical location and route of delivery, improved in vivo imaging methods are needed. These methods could also be used to guide surgeons during the encapsulated islet transplantation process and to detect post-surgical complications.[17] Magnetic resonance imaging (MRI) is the imaging modality of choice for the visualisation and tracking of non-encapsulated islet transplants. MRI offers high spatial resolution and soft-tissue contrast, and does not rely on ionizing radiation. MRI can also be used to guide the islet engraftment process using real-time visualisation.[18] Until now, most of the MRI-assisted implantations have been performed by labeling the islets with superparamagnetic iron-oxide (SPIO) nanoparticles.[19-22] This "negative" contrast agent offers the possibility to detect islets at a very high sensitivity using T_2/T_2*-weighted MRI. The visualisation of single cells is achievable using superparamagnetic iron-oxide labeling, coupled with scanning procedures relying on adequate hardware.[23] It was suggested that allograft rejection can be monitored through the use of MRI, as immunorejection leads to islet cell death and subsequent disappearance of hypointensity volumes.[24] SPIO-labelled islets were detected for at least 188 days post-engraftment into mice.[25]

Although no effects on islet viability or insulin secretion after labeling were reported in these studies, the effects of the labeling agents on long-term islet function remains a concern.

One drawback of SPIO and other T_2/T_2* "negative" contrast agents is the absence of correlation between the SPIO concentration and the MRI signal. In fact, the "dark" areas generated by SPIO in MR images, are largely magnetic susceptibility artefacts of dimensions largely exceeding the size of the implanted islets. When considering MRI of encapsulated islets, the larger size of the beads with respect to the dimensions of the islets alone would increase the susceptibility-based image artifacts induced by SPIO. In addition to this, SPIO labeling is not a valid strategy when considering implantations in or close to the liver, due to the strong iron overload in this organ for type 1 diabetic patients. This causes hypointensity of this organ in MRI images.

"Positive" contrast agents used in T_1-weighted imaging, and mainly based on paramagnetic gadolinium, offer the possibility to correlate the MR signal with the concentration of paramagnetic materials. The "hypersignal" generated by the presence of Gd^{3+} in tissues, hydrated materials or in fluids is not an image artefact: it is caused by the efficient "relaxation" of water protons binding to, and exchanging from, the available Gd^{3+} ions contained in the contrast agent.[26] To date, very few attempts to label and to track islets with Gd^{3+}-based contrast agents have been reported. One study consisted in labeling human islets with a clinical gadolinium-based agent (GdHPDO3A).[27] The viability and functionality of cells was not impaired, and the islets were visible for at least 65 days post-engraftment into immunodeficient mice. This approach is limited by the difficulty to track small islets due to the resolution range of MRI. Islet encapsulation represents an opportunity to increase the overall volume of the implant to dimensions more closely matching the resolution of MRI, and in particular clinical MRI (> 300 μm).

To limit the cytotoxicity risks inherent to the uptake of labeling agents and nanoparticles by cells, an alternative strategy for encapsulated islet transplantation in vivo monitoring is to sequester the MRI contrast agent in the encapsulation material. The most commonly used islet microencapsulation material is alginate, which offers the possibility to incorporate Gd^{3+} directly into the polymer gel network.[28] However, this strategy is expected to change the mechanical properties and the pore size distribution of the gel, which would alter the immunoisolation characteristics of the beads. A direct comparison of beads containing the contrast agents to beads without contrast agent would be challenging. As an alternative strategy, we propose to incorporate relatively large paramagnetic nanoparticles into the alginate hydrogels.

We have previously developed mesoporous silica nanoparticles (MSNs) grafted with Gd chelates (Gd-MSNs)[29-31]. These nanoparticles could be co-encapsulated with the cells in alginate beads to enable MRI tracking. The porous network of MSNs could also be used in future studies, to supplement the cells with a variety of functional molecules that could be progressively released in vivo[32]. In addition to allowing MRI tracking, the Gd-MSNs could therefore be used to deliver anti-inflammatory, angiogenic, anti-apoptotic or other factors to improve encapsulated islet survival or function.[33] In this study, we co-encapsulated pancreatic beta cells and paramagnetic Gd-MSNs (for MRI visibility) using an emulsification and internal gelation cell immobilization process.[34] We previously demonstrated that this process enables the production of high-concentration alginate beads with reduced permeability towards antibodies and the potential to reverse diabetes in allogeneic mice.[35] Here, mouse insulinoma 6 cells were used as an initial glucose-responsive beta cell model[36] to test the effects of co-encapsulated Gd-MSNs on cell survival and expansion.

EXPERIMENTAL SECTION

Materials and methods

Unless specified, all reagents were of the highest purity and ordered from Sigma Aldrich.

Synthesis of Gd-MSNs

The synthesis of MSNs was performed according to a previously reported methodology.[37] In brief, 4 g of Pluronic F127 (EO_{106}PO70EO106 BioReagent) and 1 g of CTAB (n-cetyltrimethylammonium bromide) were mixed in an aqueous solution of NH_4OH 2.9% supplemented with ethanol (volume ratio of 2.5:1). Then, 3.86 mL of TEOS (tetraethylorthosilicate, 98%) were added to the solution. After one minute of stirring, the mixture was left 24 h for aging in static conditions (room temperature). The nanoparticles were then collected by centrifugation (15300 x g, 40 min), washed with water and dried in air at 70°C. Surfactants were removed by calcination at 550°C during 5 h (Furnace 48000, Barnstead/Thermolyne oven, heating ramp of 1°C min-1, air). These particles are referred to as MSNs.

DTPA (diethylene triamine pentaacetic acid) was grafted onto the surface of MSNs as previously reported[29]. Briefly, 160 mg of DTPA dianhydride (diethylenetriaminepentaacetic dianhydride) were dissolved in 4 mL of anhydrous DMSO (dimethyl sulfoxide) under N_2 and at room temperature. After the addition of 0.068 mL APTES (3-aminopropyl)triethoxysilane), the solution was stirred overnight. Four (4) mL of this solution were added to a suspension of MSN in anhydrous toluene (200 mL at 10 mg mL^{-1}) and the mixture was left overnight at 110 °C under $N_{2.}$ The nanoparticles were sequentially washed with 95% ethanol and then nanopure water (18.2 M, NanoPure Diamond, Barnstead, MA, USA) followed by centrifugation (7500 x g, 10 min) and vacuum-dried at 40 °C. These particles are referred to as DTPA-MSNs.

DTPA-MSNs were suspended in a 100 mM solution of gadolinium acetate ($Gd(CH_3CO_2),xH_2O$) during 1 h at room temperature, at a concentration of 10 mg mL^{-1}. The solution was vortexed 30 min, followed by 30 min in ultrasonic bath (3x), and then 16 to 24 h dialysis (1:1000 sample-to-water ratio, 1000 kDa MWCO, Spectra/Por, in deionized water, at least 4 changes). The dialysed nanoparticles were collected by centrifugation (24,000 x g, 15 min). For the experiments without cells, the nanoparticles were re-suspended in phosphate-buffered saline solution (with Ca^{2+} and and Mg^{2+}, Thermo Fisher Scientific, Walthman, MA, USA) supplemented with 10 % FBS (Fetal Bovine Serum, Thermo Fisher Scientific, Walthman, MA, USA). For the cell-containing experiments, the nanoparticles were re-suspended in DMEM cell culture medium supplemented with 10% FBS and 1% penicillin-streptomycin (all from Thermo Fisher Scientific). In both cases, MSNs were resuspended at a starting concentration of 50 mg mL^{-1} (initial mass of powder suspended in fluid). The suspensions were vortexed and sonicated (3 times 30 min), then centrifuged (500 x g for 5 min.) to remove possible aggregates. The supernatant was collected and will be referred to as Gd-MSNs. The gadolinium concentration in these solutions was assessed by neutron activation analysis (see next section). For cell culture experiments, Gd-MSNs solutions were gamma-irradiated (1 h, final dose of 25 kGy ± 10 %; Nordion, Gamma Center of Excellence, Laval, Canada) prior to cell encapsulation.

Characterization of MSNs

Textural analysis: The textural properties of MSNs were measured by low-angle X-ray diffraction (XRD), nitrogen physisorption measurements, as well as thermal differential analysis (TGA). These results are described in the Supporting Information section.

Transmission electron microscopy (TEM): The size distribution of MSNs was measured by transmission electron microscopy (Jeol JEM-1230, 80 keV, Tokyo, Japan). The particles were dispersed in water, deposited on a carbon-coated copper grid (CF3000-Cu, Electron Microscopy Sciences, Hatfield, PA, USA) and then imaged. The size distribution of at least 125 particles (on 3 different images taken at 3 different locations) was determined using the ImageJ software.[38]

Dynamic Light Scattering (DLS): The hydrodynamic diameter and colloidal stability of the particles suspension in complete medium were assessed by DLS with a Nano S Zetasizer system (Malvern Instruments, Worcestershire, UK.) using a laser (He-Ne) wavelength of 633 nm and a scattering angle of 173°. The temperature measurement was fixed at 25° C. The viscosity and the refractive index were set respectively to 0.940 cP and 1.345, for DMEM with 10% FBS.[39] For silica nanoparticles, the refractive index was set to 1.45. The hydrodynamic diameter was calculated from the average of three measurements.

Neutron activation analysis (NAA): NAA was used to quantify the gadolinium concentration of the nanoparticle suspensions at the end of the suspension process. PCR tubes of 0.2 mL containing the suspension of Gd-MSN in complete medium were inserted in a Slowpoke reactor (20 kW, Ecole Polytechnique, Montréal, Canada), and analysed as previously reported.[40]

Relaxivity measurements: The relaxometric properties of the concentrated Gd-MSNs suspensions were evaluated by measuring their longitudinal and transversal ^{1}H proton relaxation times (T_1 and T_2) with a time-domain nuclear magnetic resonance relaxometer (Bruker Minispec, 60 mq, 60 MHz (1.41 T), 37 °C, 300 µL of solution in 7 mm NRM tubes). For the measurement of T_1, a standard inversion-recovery sequence was used with 15 different delays. For T_2 measurements, a standard Carr-Purcell-Meibom-Gill sequence was used with at least 12 echos. The Gd-MSN stock solution synthesized for the production of alginate beads without cells had a T_1 of 12.9 ms, a T_2 of 7.9 ms and a Gd concentration of 3.71 mM; the stock synthesized for the production of alginate beads with cells had a T_1 of 26.6 ms, a T_2 of 14.2 ms, and a Gd concentration of 3.65 mM.

X-ray diffraction, thermogravimetric analysis and nitrogen physisorption: These methods are detailed in the Supporting Information section (supplementary materials & methods).

Mouse insulinoma 6 cell culture

MIN6 cells (kind gift from James D. Johnson, UBC) were cultured in complete medium, consisting of DMEM supplemented with 10% fetal bovine serum, 1% penicillin/streptomycin, 2 mM final concentration L-Glutamine (all from Thermo Fisher Scientific), and 5 mM beta mercaptoethanol. Adherent non-encapsulated MIN6 cells were cultured in surface treated T-flasks (Sarstedt) with at a seeding density of approximately 5 x 10^4 cells/cm^2 in 20 mL/75 cm^2 complete medium. Cells were enumerated using a hemocytometer after Trypan Blue staining (0.2% in phosphate-buffered saline solution, Fisher Scientific). Complete media changes were performed every 2 to 3 days. The cells were passaged when reaching approximately 90% confluency (5 x 10^5 cells/cm^2) by rinsing with phosphate-buffered saline solution (Ca^{2+} and Mg^{2+} free, Thermo Fisher Scientific), then incubating the cell culture in TrypLE (Thermo Fisher Scientific) at 37°C and 5% CO_2 for 5 min. Detached cultures were centrifuged at 350 x g then resuspended in complete medium at the desired concentration. To generate the cell seed stock for encapsulation, suspended cells were washed in complete medium, enumerated after Trypan Blue staining and then re-suspended at 10.5 x 10^6 cell/mL to obtain a final concentration of 10^6 cells/mL beads. After encapsulation, the immobilized cells were cultured in untreated 25 cm^2 T-flasks (Sarstedt) by adding 1 mL beads to 9 mL complete medium. Every second day, half of the medium was exchanged by adding 10 mL complete medium to each T-Flask, mixing, placing the flask with the vent facing upward, allowing the beads to settle, and then aspirating medium in excess of 10 mL total volume.

Gd-MSN and/or cell immobilization by emulsification and internal gelation

Preparation of solutions and reagents: The emulsification and internal gelation process buffer consisted in 10 mM HEPES (4-(2-hy droxy ethy l)-1-piperazineethanesulfonic acid) and 170 mM NaCl (both from Thermo Fisher Scientific) at pH 7.4, as previously described [34-35]. The alginate stock solution was prepared by adding sodium alginate (Sigma-Aldrich, CAS Number 9005-38-3, Medium Viscosity) at the concentration required to obtain 2% alginate concentration in the final alginate suspension containing $CaCO_3$, Gd-MSNs and/or cells. After overnight dissolution in a stirred vessel, the alginate solution was autoclaved for 30 min (excluding ramp up and down time) at 122.5 °C and 16.8 psig. The $CaCO_3$ suspension was prepared by adding 500 mM $CaCO_3$ powder (Sigma-Aldrich) to the HEPES process buffer, followed by autoclaving. The acidified oil solution was prepared immediately prior to the emulsification and internal gelation process by adding 44.5 µL glacial acetic acid to 11 mL of mineral oil (both from Thermo Fisher Scientific) in a 50 mL conical tube (Sarstedt, Nümbrecht, Germany), and vortexing the mixture until complete acid dissolution.

For experiments without cells, an alginate/$CaCO_3$/Gd-MSN suspension was prepared by mixing alginate stock solution, $CaCO_3$ suspension, and complete medium at 18:1:1:1 volumetric ratio (for example, 9.9 mL alginate solution, 0.55 mL Gd-MSN suspension, 0.55 mL $CaCO_3$ suspension and 0.55 mL complete medium). For experiments with cells, an alginate/$CaCO_3$/Gd-MSN/cell suspension was prepared by mixing alginate stock solution, Gd-MSN suspension, $CaCO_3$ suspension, and MIN6 cells in complete medium at 16:2:1:2 volumetric ratio (for example, 8.8 mL alginate solution, 1.1 mL Gd-MSN suspension, 0.55 mL $CaCO_3$ suspension and 1.1 mL cell stock solution). To obtain controls without Gd-MSNs, the volume of Gd-MSN suspension was replaced by complete medium.

Emulsification and internal gelation process: The emulsion process was performed as previously described[34-35, 41]. After preparing the alginate/$CaCO_3$ suspension with or without Gd-MSNs and/or cells, 20 mL light mineral oil (There Fisher Scientific) was added to a spinner flask (Bellco Glass, Vineland, NJ, USA). Using a syringe (VWR, Radnor, PA, USA), 10 mL of the alginate suspension (with or without Gd-MSNs and/or cells) was added to the mineral oil, dropwise. The mixture was agitated at 486 rpm to generate an alginate-in-oil emulsion. This agitation rate (N_i) was selected based on the target volume area moment mean diameter (De Brouckere mean diameter, D_{43}), based on the relationship between D_{43} and N_i, determined beforehand as described previously.[34, 41] Before the 12 min mark was reached, the acidified oil solution was prepared. At the 12 min mark, 11 mL of the acidified oil solution was added to the spinner flask to trigger internal gelation. At the 13.5 min mark, the agitation rate was decreased to 200 rpm. At the 20 min mark, 40 mL of HEPES process buffer supplemented with 10% complete medium was added to the spinner flask to neutralize the acid. At 21.5 min, the agitation was stopped. Using a 50 mL large bore pipette (Thermo Fisher Scientific), the contents of the flask were aspirated and transferred into two 50 mL conical tubes (Sarstedt). The tubes were centrifuged for 3 min at 630 x g to accelerate phase separation. Most of the organic and aqueous phases were aspirated while carefully avoiding bead aspiration. An additional 30 mL of complete medium was added to each centrifuge tube to remove most of the oil by repeating the centrifugation and aspiration process. The beads were then filtered on a 40 μm cell strainer (Thermo Fisher Scientific) and transferred into HEPES process buffer at 1:5 volumetric ratio (beads:total volume) for MRI or bead size distribution analysis. Alternatively, for cell culture, the beads were transferred into complete cell culture medium at 1:10 volumetric ratio and then transferred into suspension culture vented T-flasks (Sarstedt).

Bead size distribution measurement

To determine the size distribution of the alginate beads, 1 mL beads were transferred into a 15 mL conical tube (Sarstedt) containing 4 mL HEPES process buffer supplemented with 10% complete medium. A saturated Toluidine Blue O solution was prepared in HEPES process buffer, and 100 μL of this solution were added to the bead suspension. The tubes were incubated for 1 h at room temperature on an orbital shaker at 50 rpm. The stained bead suspension was transferred into a 10 cm Petri dish (Thermo Fisher Scientific), and an additional 5 mL of HEPES process buffer with 10% complete medium was added to the dish. A ruler was placed next to the dish, and an image was acquired using a Samsung Glaxy S4 13 MP handheld camera. The bead sizes were determined by image analysis using CellProfiler freeware[42].

MRI assessment of Gd-MSN retention in alginate beads

MRI was used to assess the total retention of Gd-MSNs in the polymer beads, as indicated by the total MRI signal produced by the beads imaged with a T_1-weighted MRI sequence. MRI is a powerful technique to detect the presence of low concentrations of paramagnetic elements (e.g. gadolinium); the occurrence of Gd^{3+}, Gd-DTPA, or Gd-DTPA-MSNs potentially escaping the alginate network, would be efficiently detected in T_1-weighted MRI down to concentrations of 0.05 mM (Gd).

Cell-free beads: First, 40 µL beads were distributed into the wells of a 96-well plate. To do so, a 1 mL pipette with a cut tip was used to aspirate 0.2 mL of bead suspension in HEPES process buffer (1:5 beads:total volume ratio) while manually mixing the suspension to avoid bead settling during pipetting. The plate was then inserted in a radiofrequency coil adapted to scanning 96-well plates. The plates were scanned with a 1-Tesla MRI (M2M, Aspect Imaging, Netanya, Israel). A T_1-weighted 2D spin echo sequence was used with the following parameters: TE = 11.2 ms; TR = 400, 700, 1000 ms; slice/interslice = 1.5/0.1; FOV: 70 mm; matrix: 200 x 200; 3 NEX; acquisition time: 4.0 min. The beads were scanned 24 h after alginate bead preparation, and then 5 months later (slight adjustment at TE = 13.3 and slice thickness of 0.5). The samples were kept at 4ºC between the scans. For the 24 h MRI scans, contrast enhancement was calculated based on the comparison of the signal produced by the beads, to that produced by controls (nanopure water), as follows:

$$Contrast\ enhancement = \frac{2 \times \left(I_{sample} - I_{control}\right)}{I_{sample} + I_{control}} \qquad \textbf{Eq. 1}$$

Intensities (I) were measured by defining 20 pixel regions of interest in the center of each image (Image J software). The average of intensity values was calculated, as well as the corresponding standard deviation. Results from the long-term follow-up scan (t = 5 months) were compared with the initial scan (t = 24 h) by calculating the intensity ratio between each alginate bead sample and its corresponding supernatant.

Cell-containing beads: Samples of cell-containing beads were processed and scanned after 24 h and 5 months. Here, the bead:total volume ratio was 1:10, resulting in 20 µL/well bead sample volumes. Between scans, the cell-containing beads were kept in T-75 flasks in a cell incubator (standard condition). The cell culture medium was refreshed every 48 h to 72 h for the first 14 days. Prior to each scan, samples of beads were freshly deposited in 96-well plates (time points:

24 h, 48 h, 72 h, 14 days, 1 month and 2 months), and MRI images were acquired as described above. The retention of Gd-MSNs inside the alginate beads was confirmed by measuring the ratio between signal in the beads and the signal in the supernatant. Any decrease in this ratio would indicate a release of the gadolinium into the medium.

Live/dead staining of immobilized cells

A live/dead staining solution consisting of HEPES process buffer supplemented with 10% complete medium, 4 μM calcein AM, 4 μM ethidium homodimer and 4 mM Hoechst (all from Thermo Fisher Scientific) was prepared. Dead cell controls were obtained by filtering the beads using a 40 μm nylon cell strainer, and transferring beads into a microcentrifuge tube containing 1 mL of 99% ethanol prior to live/dead staining. Sample or control beads were then transferred into the staining solution at 1:5 bead:total volume ratio. The mixture was incubated for 30 min at room temperature in the dark. The beads were rinsed with HEPES process buffer supplemented with 10% complete medium and imaged using a fluorescence microscope (Olympus IX81, Tokyo, Japan, model: IX2).

Bead degelling and packed cell volume measurements

A degelling solution consisting in 55 mM citrate (Thermo Fisher Scientific), 10 mM HEPES, 95 mM NaCl, at pH 7.4 was prepared. Cells were liberated from the alginate beads by placing 1 volume of the beads in 9 volumes of 90% degelling solution with 10% complete medium and incubating on ice on a rotary shaker at 50 rpm for 20 min. For packed cell volume measurements, 1 mL of the degelled mixture was pipetted into packed cell volume tubes (TPP Techno Plastic Products AG, Switzerland) followed by centrifugation at 2500 x g for 2 min.

Quantitative polymerase chain reaction (q-PCR)

After degelling the beads as described above, 1 mL of the degelled mixture was placed in an RNase-free microcentrifuge tube and the cells were washed once in phosphate-buffered saline solution. After adding 350 µL RLT buffer (Qiagen, Hilden, Germany) per tube, samples were stored at -80ºC. RNA was extracted from the MIN6 cells using the RNeasy Mini Kit (Qiagen, Hilden, Germany). Reverse transcription qPCR was performed on the extracted RNA for (mouse) insulin I (*Ins1*), insulin II (*Ins2*), pancreas/duodenum homebox protein 1 (*Pdx1*), Glucose Transporter 2 (*Glut2*), homeobox protein Nkx-6.1 (*NKX6-1*), beta-actin (*ActB*) and glyceraldehyde 3-phosphate dehydrogenase (*Gapdh*). Table S1 details the primer sequences used for qPCR. The Viia7 qPCR instrument (Thermo Fisher Scientific) was used to detect the amplification level and was programmed with an initial step of 20 sec at 95˚C, followed by 40 cycles of 1 sec at 95˚C and 20 sec at 60˚C. Relative expression was calculated using the Expression Suite software (Thermo Fisher Scientific).

Statistics

For the results of cell studies, two-way equivalency comparisons of the slopes and intercepts of different linear functions were performed using 2-tailed t-tests for independent samples. The F-test was used to validate the significance of regression of linear regression fits, all in Prism 5 (GraphPad, San Diego, California). Unless otherwise mentioned, results represent the experimental average ± the standard error of the mean. For qPCR experiments, changes in gene expression were analyzed by ANOVA testing followed by Fisher's least significant difference test. Results were considered to be statistically significant at $p < 0.05$.

Results

Synthesis and characterization of Gd-MSNs

The MSNs were synthesized with a well-established Stöber modified method[29, 37] leading to spherical nanoparticles (Figure 1 - a,b). The size distribution (Figure 1 b) revealed a distribution centered at 166 nm ± 22 nm (full width of peak at half maximum - FWHM), similar to other results reported in the literature for this synthesis procedure.[29, 37, 43-44] The X-ray diffraction pattern revealed particles of a MCM-48 porosity network (Figure S1 in the Supporting Information).[45] The nitrogen physisorption results indicated open porosity even after complexation with Gd-DTPA (Table S2 in the Supporting Information). The number-weighted and intensity-weighted hydrodynamic diameter profiles measured by DLS in water, are plotted in Figure 1-c (intensity: 246 ± 9 nm FWHM; number: 195 ± 8 nm FWHM). MSNs appeared to be well-dispersed and non-aggregated. No significant difference was found between nanoparticles measured on the day of preparation, after 3 days in suspension (after slight agitation), and after gamma irradiation prior to encapsulation.

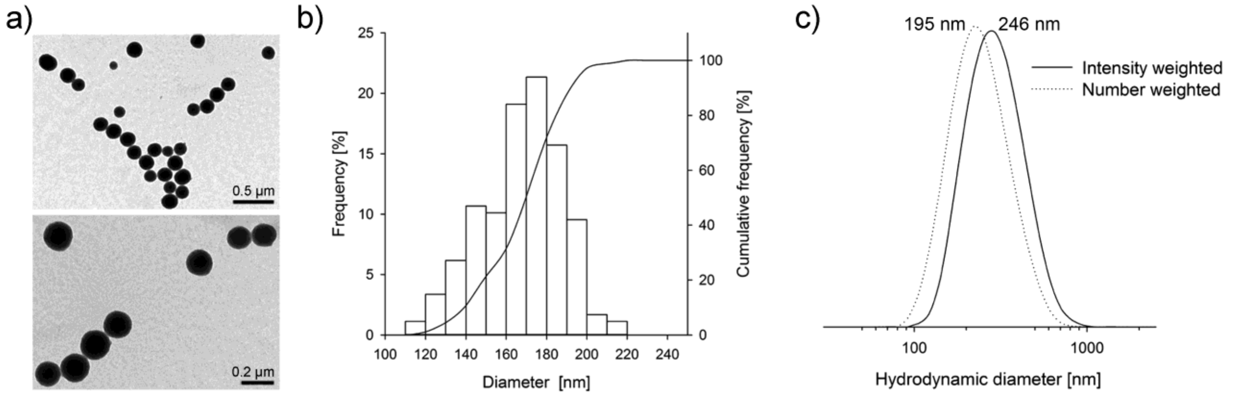

Figure 1. Size characterisation of Gd-MSNs: a) TEM images; b) corresponding particle size distribution; c) hydrodynamic size by DLS.

Relaxometric and MRI contrast-enhancement properties of Gd-MSNs

Relaxation times were measured at different gadolinium concentrations (Figure 2-a), and the results were plotted in the form of a relaxometric graph. The slope of $1/T_1$ and $1/T_2$ provided the relaxivity values r_1 and r_2, respectively (r_1 = 29 mM^{-1} s^{-1} and a r_2 = 42 mM^{-1} s^{-1}, r_2/r_1 of 1.45), typical of a high-performance “positive” contrast agent when scanning under T_1-weighted MRI sequences. These values are similar to those obtained with other Gd-MSNs nanoparticle systems published recently.[29] The theoretical signal expected when using T_1-w. spin echo sequences can be calculated by using the following equation:

$$S \propto \rho_H \left(1 - e^{-TR/T_1}\right)\left(e^{-TE/T_2}\right) \qquad \text{Equation 2}$$

where ρ_H is the density of protons, TR is the repetition time, TE the echo time, and T_1 and T_2 are the longitudinal and transverse relaxation times measured for a given contrast agent. Figure 2-b represents the simulated signal intensity calculated using Equation 2 as well as T_1 and T_2 values measured at each concentration time. At low concentration the signal intensity rises drastically, then reaches a peak at about 0.25 mM – 0.4 mM, followed by a progressive decrease. The simulated signal intensity curve indicates the maximum signal that can be achieved with a T_1-weighted spin-echo sequence (TE/TR = 10/400 ms). According to this curve, a concentration of 0.15 – 0.5 mM of gadolinium (Gd-MSNs) dispersed in the volume of the alginate beads would lead to an optimal signal enhancement once visualised in T_1-w. MRI. The theoretical signal intensity curve was confirmed by measuring with MRI (Figure 2.c: TE/TR = 11.2/400 ms), the signal of samples of the contrast agent at different concentrations. The highest signal intensity occurred at a concentration of 0.239 mM and significant signal enhancement was revealed at concentrations as low as 0.016 mM Gd.

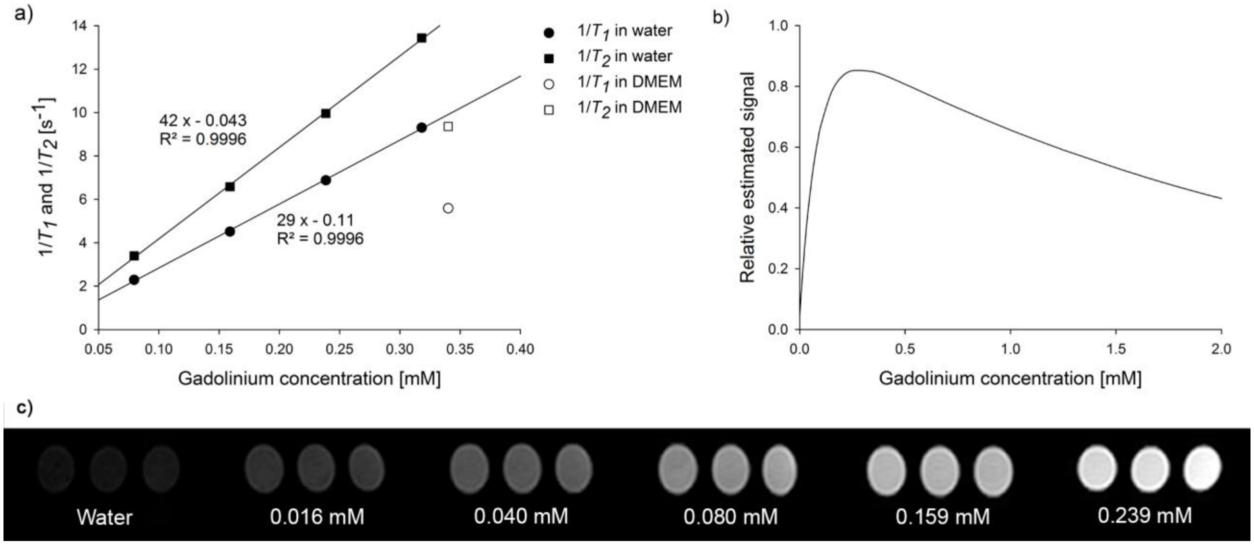

Figure 2. Relaxometric measurements of Gd-MSNs in water: a) relaxometric curves (1/T_1, 1/T_2); b) MRI signal enhancement curves based on r_1 and r_2 (measured), and spin-echo parameters TE = 10 ms and TR = 400 ms) and c) contrast provided in MRI, by the Gd-MSNs suspensions scanned under the same parameters.

Alginate beads, Gd-MSN retention and MRI contrast-enhancement properties

Figure 3 shows the volumetric fraction and cumulative volume fraction as a function of the bead diameter obtained from the emulsification and internal gelation alginate bead production process. At the 486 rpm agitation rate used during the emulsification step, the average bead diameter (D_{21}) was 505 ± 427 µm (standard deviation), the surface area moment mean diameter (Sauter mean diameter, D_{32}) was 867 ± 565 µm (area-weighed standard deviation), and D_{43} was 1235 ± 662 µm (volume-weighed standard deviation). The broad bead size distribution obtained is expected for stirred emulsification-based alginate bead production.[34] The D_{43} obtained may lead to oxygen mass transfer limitations in vivo but should not be problematic for the current in vitro study.[46] For in vivo applications, the agitation rate should be increased to obtain slightly smaller beads.

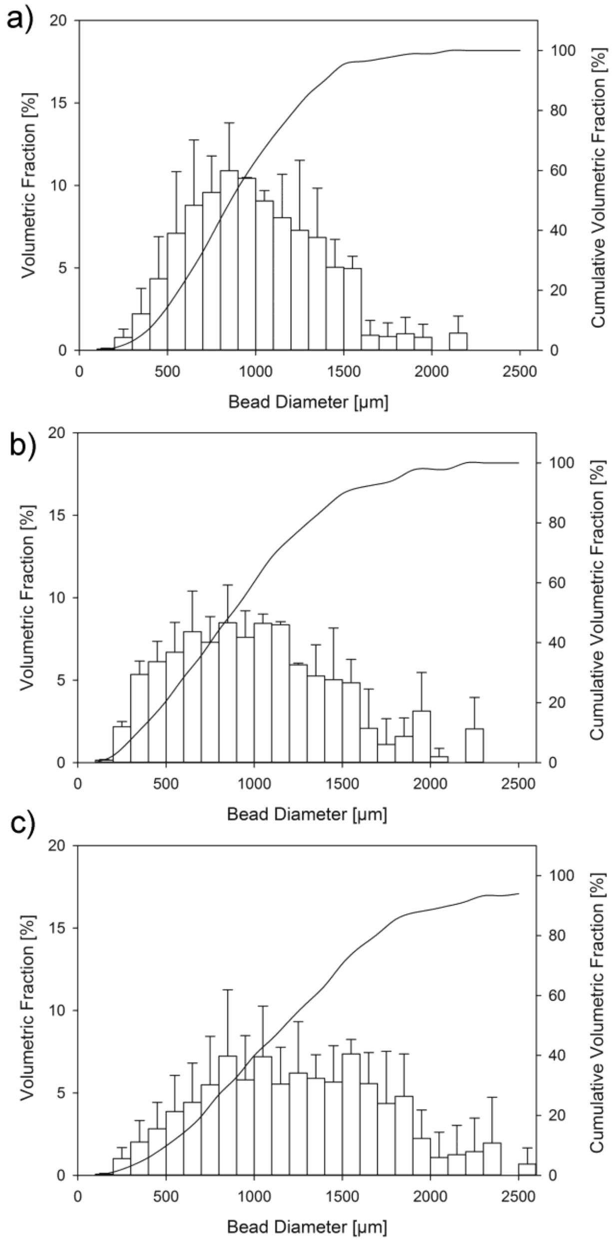

Figure 3. Size-distribution of alginate beads with a) Gd:MSNs only; b) cells only; c) Gd:MSNs and cells.

Figure 2.b was used as a guideline for the preparation of alginate beads containing a Gd concentration enabling MRI contrast enhancement. For the Gd-MSNs retention assay, a Gd-MSN suspension of 3.71 mM was used, and diluted at a factor of 12 with the other products of alginate preparation. This would theoretically lead to a Gd concentration of 0.31 mM, which is very close to the value expected from the signal-enhancement peak indicated by Figure 2.b.

For MRI visualization, alginate beads containing Gd-MSNs were suspended in two different buffers (complete medium or HEPES buffer + 10% complete medium). They were MRI-scanned using a T_1-weighted spin echo sequence performed at three different repetition times (TR = 400, 700, and 1000 ms; see Figure 4). The beads were scanned 24 h after preparation (Figure 4.a), and then at 5 months (Figure 4.b). No significant difference in signal was found between nanopure water and control beads without nanoparticles (in complete medium or in HEPES process buffer + 10% complete medium).

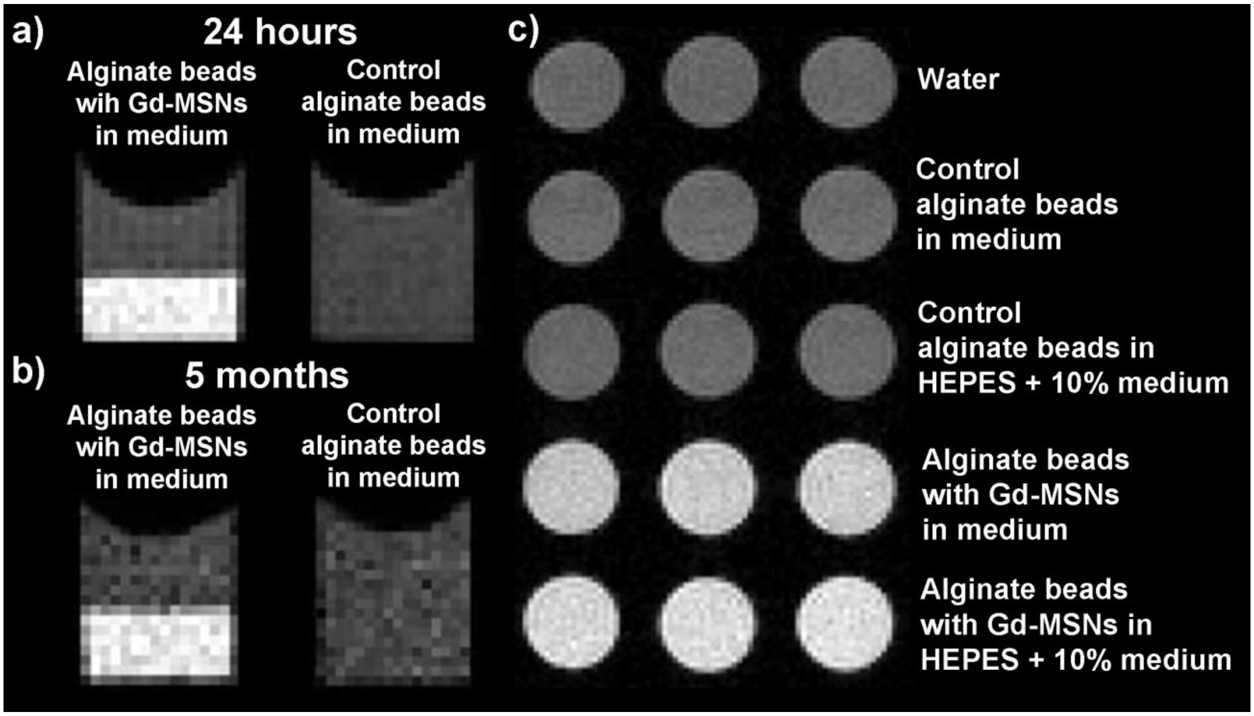

Figure 4. T_1-w. MRI images (TE/TR = 11.2-13.3/400 ms) of Gd-MSNs-containing 2% alginate beads 24h after the emulsion process (a), and after 5 months (b). Images at t = 24h were acquired with a slice thickness of 1.5 mm, whereas those at t = 5 months were acquired with a slice thickness of 0.5 mm (noisier). Controls (alginate beads without Gd-MSNs) are provided at the right side. In (c): coronal images of water, controls, and Gd-MSNs-containing beads, in both complete medium and HEPES buffer + 10% complete medium (no difference in signal was noted between the buffers).

The intensity generated by the beads in each condition, as well as the contrast calculated based on the comparison with the signal of nanopure water (control), are presented in Table 1. As expected, longer repetition times lead to images generated with much more signal and thus lower signal-to-noise ratios. The contrast of Gd-MSNs-containing beads compared with the control, appeared to be 82.7% or 96.4%, respectively for beads suspended in complete medium or in HEPES buffer + 10% complete medium (at TR = 400 ms; condition of maximal contrast). A slightly higher signal was found for alginate beads with Gd-MSNs suspended in HEPES buffer + 10% complete medium, compared with complete medium alone. This difference could be due to the presence of serum proteins in the complete medium that was used for the experiment. The preparation of beads in complete medium might lead to protein adsorption to the bead and or bead pore surfaces, which could slightly affect the free circulation and binding of H_2O to the Gd^{3+} paramagnetic sites. The contrast between controls (alginate only) and nanopure water was not significant. No significant difference was found between control beads (without Gd-MSNs) scanned in HEPES buffer + 10% complete medium and those scanned in complete medium. Overall, these results confirm that the presence of ~ 0.31 mM Gd in the alginate beads leads to a strong signal enhancement in T_1-w. images. In all conditions, the error on the intensity measurement and on the calculated contrast values gradually decreased with increasing TR values due to the stronger signal detected. Five months later, the same samples were scanned in MRI with a TR of 400 ms, since this was the condition leading to the best contrast enhancement. The contrast enhancement with regards to the control beads was 86% in complete medium and 108% in HEPES buffer + 10% medium with respect to the control beads. The increase between the value at 24 h and 5 months (3.6% for complete medium and 11.7% for HEPES buffer + 10% complete medium) could be explained by a slight concentration of the Gd contents due either to the contraction of the alginate network, or by evaporation of a certain quantity of the water from the wells, potentially leading to a local Gd concentration increase in the beads. Overall these changes are not drastic, and would not impede the identification of Gd-MSN-alginate beads in vivo. These results also confirm the strong and stable entrapment of Gd-MSNs in the alginate network, since the leaching of even a slight concentration of Gd-containing product from the polymer network (e.g. sub- 0.05 mM) would have been detectable in MRI.

Table 1. MRI signal intensity and contrast enhancement obtained with 2% alginate beads supplemented with Gd-MSNs.[a]

Sample	Medium	Repetition time (TR) in T_1-w. MRI [ms]	Intensity (average of 3 samples)	Standard. deviation (+/-)	Relative error (std.dev./int.) [%]	Contrast [%]	Absolute Error (+/-) [%]	Relative Error [%]
Gd-MSNs beads	Complete medium	400	8161	180	2.20	82.7	1.54	0.02
Gd-MSNs beads	Complete medium	700	11503	262	2.28	69.5	0.95	0.01
Gd-MSNs beads	Complete medium	1000	13573	69	1.95	61.1	1.57	0.03
Gd-MSNs beads	HEPES buffer +10% medium	400	9804	170	1.73	96.4	1.02	0.01
Gd-MSNs beads	HEPES buffer +10% medium	700	13135	221	1.68	83.2	0.49	0.01
Gd-MSNs beads	HEPES buffer +10% medium	1000	14864	264	1.81	69.5	0.71	0.01

[a]The contrast is the % of signal increase compared to controls. The signal intensity results obtained for controls (cell-free beads without nanoparticles and nanopure water) are provided in Table S3 of the Supporting Information.

Alginate beads with cells: MRI contrast-enhancement properties

Alginate beads containing cells were produced and MRI-scanned over a period of several days. Beads with Gd-MSNs were clearly visible (Figure 5. c,d), even with a bead quantity reduced to 20 µL/well compared to prior cell-free beads imaged at ~100 µL/well (Figure 4). The signal was measured, and the contrast enhancement was calculated with respect to water and in function of the time of scanning (Figure 5, e). For the beads with Gd-MSNs (Figure 5 c and d) the gadolinium concentration was 0.34 mM (optimal range for contrast enhancement, as revealed in Figure 2 b). The beads appeared distinctly contrasted, corroborating the Gd-MSNs visualisation in Figure 2 c. The evolution of contrast was monitored over a period of over 2 months. The general evolution of the curves was similar for all the samples, indicating the occurrence of little deviations due to experimental variations during the imaging (e.g. temperature). For the alginate beads with Gd-MSNs, with or without cells, the contrast enhancement was between 55% and 65%. Beads synthesized with cells only (without Gd-MSNs) had a contrast enhancement of 0% ± 4% (experimental error) with respect to nanopure water. This confirms that Gd-DTPA functions grafted at the surface of MSNs remain in the silica structures, which are in turn entrapped into the alginate beads. There was no evidence of Gd-MSN leaching from the gel, making Gd-MSN internalisation by the cells unlikely, except potentially for Gd-MSNs in direct contact with the cells. Finally, a 2-fold contrast enhancement was noted between the Gd-MSN alginate beads compared with free suspensions of Gd-MSNs (without alginate). This phenomenon could be explained by the restricted access of water to the Gd^{3+} groups in a polymeric structure such as alginate.[47]

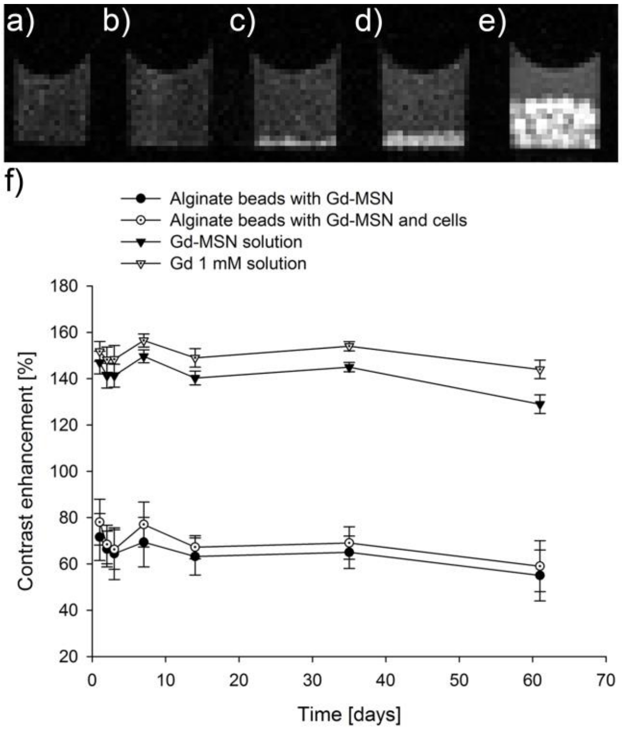

Figure 5. Entrapment of Gd-MSNs in alginate beads. MRI in vitro visualization assays of paramagnetic alginate beads: a) water, b) alginate beads with cells, c) alginate beads with Gd:MSN, d) alginate beads with cells and Gd:MSN and e) long-term follow-up of contrast enhancement of the beads placed in complete medium.

Effect of Gd-MSNs on MIN6 cell survival and expansion

The MIN6 cells used in these experiments are an immortalized cell line that is expected to expand to form aggregates in alginate.[48] As a first indication of potential Gd-MSN effects on beta cells, MIN6 cells were encapsulated in alginate beads with or without co-encapsulated Gd-MSNs. The effect of the Gd-MSNs on MIN6 cell survival was determined by live/dead staining the day following the encapsulation process and at regular intervals during cell expansion. The cell growth rate and lag time before reaching exponential growth were used as an indication of cellular health and metabolic function.

One day after encapsulation, very few dead cells were observed within the beads (Figure 6). One week after the encapsulation, the majority of cells remained alive, whether encapsulated with or without Gd-MSNs. On day 14, reduced cell densities were observed for MIN6 cells co-encapsulated with Gd-MSNs compared to cells encapsulated without Gd-MSNs (Figure 6). As expected, MIN6 cells encapsulated as single cells in alginate beads grew to form ~150 µm diameter clusters after 14 days of immobilized culture.[34, 49]

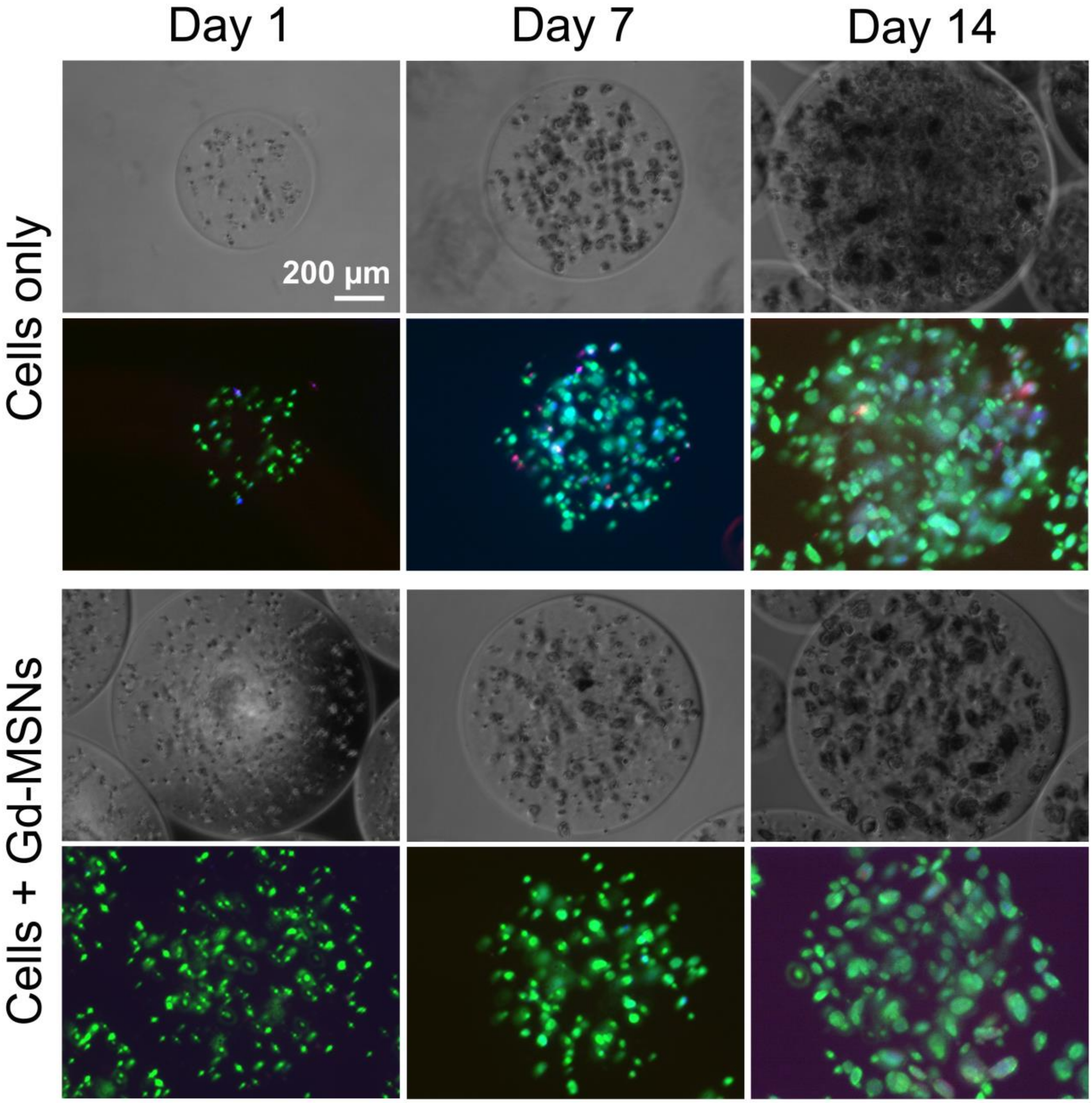

Figure 6. Imaging of the MIN6 cells grown with and without the Gd-MSNs. The black and white images are phase contrast images taken at 4x magnification. The colour images are live/dead (green, i.e. calcein AM positive / red, i.e. ethidium homodimer positive) fluorescence micrographs taken at the same field of view.

Based on packed cell volume measurements (Figure 7), the cell doubling time was 4.5 ± 0.5 days without significant lag time for MIN6 cells encapsulated alone, while MIN6 co-encapsulated with Gd-MSNs exhibited a doubling time of 5.0 ± 0.3 days with a lag time of 2.0 ± 0.8 days. Due to the experimental complexity associated with co-encapsulation, the Gd-MSNs were seeded 4, 5 and 6 hours after detachment from adherent culture, whereas the cells without Gd-MSNs were seeded 1, 2, and 3 hours after detachment. The statistically significant increase in the lag time for the MIN6 cells co-encapsulated with Gd-MSNs could thus be due either to the time interval between cell detachment and encapsulation, or to the presence of the Gd-MSNs. Future work will aim to decouple the effect of the time between cell detachment and encapsulation from the effect of the Gd-MSNs on the cell lag time.

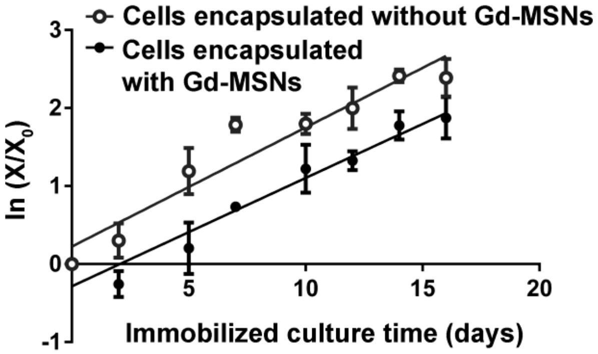

Figure 7. Growth curves of immobilized MIN6 cells with (closed circles) or without (open circles) co-encapsulated Gd-MSNs. X represents the cell concentration at time *t*; X_0 represents the initial cell concentration (both measured in packed cell volume/mL alginate).

Effect of co-encapsulated Gd-MSNs on MIN6 gene expression

Finally, the effect of the Gd-MSNs on beta cell gene expression was studied as a preliminary functional assessment. The expression of genes involved in glucose uptake and insulin secretion (*Ins1*, *Ins2*, *Pdx1*, *Glut2*, *NKX6-1*) was quantified relative to housekeeping genes (*ActB* and *Gapdh*) 1, 7 or 14 days post-encapsulation. No significant change in the expression of one housekeeping gene relative to the other were noted. Moreover, no significant changes in gene expression were observed during immobilized culture with or without Gd-MSNs for any of the genes related to glucose-responsive insulin secretion, aside from *Glut2*. For *Glut2*, a 1.38 ± 0.18 fold increase in gene expression relative to *ActB* was observed after 14 days of immobilized culture in the presence of Gd-MSNs (Figure 8).

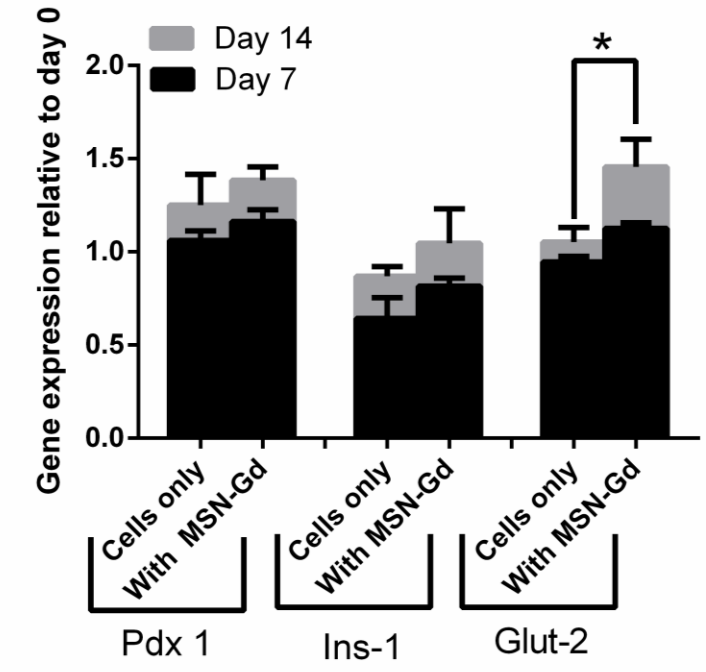

Figure 8. Change in *Pdx1*, *Ins1* and *Glu2* gene expression normalized to *ActB* as a function of time and Gd-MSNs. Values are reported relative to the expression of the same gene before encapsulation or Gd-MSN addition. *p < 0.05.

Discussion

Islet microencapsulation is a promising approach to limit or even overcome the need for immune suppression following islet transplantation. The most common encapsulated islet transplantation site is the peritoneal cavity due to the relatively large graft volume currently required. However, bead movement and agglomeration in the peritoneal space may exacerbate mass transfer limitations, particularly in bipeds.[16] For humans, the minimum graft volume required to transplant ~1 million islets encapsulated in ~600 μm diameter beads with 1 islet/bead would be 113 mL. Developing imaging techniques and tools to track transplanted encapsulated cells is pivotal to monitoring bead distribution and settling in vivo, as well as understanding potential causes of encapsulated islet cell death.

MRI is possibly the best noninvasive imaging technique to track implanted islets.[50-52] This high-resolution whole-body imaging modality allows very good soft tissue contrast. Contrary to computed X-ray tomography, MRI does not use ionizing radiation. Hence, MRI would enable multiple and repeated scans on the same patient. Until now, attempts to track islets were mainly performed by using "negative" contrast agents coupled with T_2-weighted MRI.[18, 22, 53-54] In general, negative contrast agents such as iron oxide nanoparticles provide higher detection sensitivity for cell labeling, compared with Gd^{3+}-based ones (“positive” contrast agents). However, iron oxide nanoparticles generate “blooming artifacts” which can severely impede the delineation of anatomical information. It is often difficult to differentiate between the signal loss generated by iron oxide nanoparticles and that generated by calcified tissues or by the agglomeration of magnetic substances such as blood clots.[55]

Because they generate a signal increase, Gd^{3+}-based contrast agents could be used with T_1-weighted MRI sequences to track islets with a higher precision, in spite of a lower sensitivity. Biancone *et al.*[56] visualized islets in the mouse by MRI. For this, the cells were labeled with gadolinium contrast agent (GdHPDO3A) prior to implantation. This study provided the first demonstration of islet detection using a "positive" contrast agent. However, only limited concentrations of Gd can be taken up by cells using such a small Gd^{3+}-based imaging probe. Moreover, once internalised by cells, the amount of free water available to generate the chemical exchange cascade leading to T_1 relaxation is too low, which considerably restricts the possibility to achieve full signal enhancement (as predicted by Figure 2.b).[57] Finally, the elimination of contrast agent from the cells limits the capacity for long-term graft monitoring. The present strategy, which consists in the sequestration of Gd-grafted nanoparticles inside the alginate immune-protective capsule surrounding the islets, provides an optimal interaction between the Gd^{3+} moieties and the free water diffusing into the alginate network. As a result, a larger concentration of Gd^{3+} can be distributed outside and around cells, leading to a much stronger positive signal. This approach also avoids limitations related to contrast agent exocytosis observed in direct cell labeling strategies. Finally, the larger size of alginate beads compared to cells facilitates the detection of the paramagnetic implants compared to the detection of islets alone. Arifin *et al.* were the first to report MRI of microencapsulated islets while adding a contrast agent to the alginate.[58] In their study, the contrast agent consisted in gold nanoparticles functionalized with gadolinium chelates. The present work explores this concept further by using nanoparticles of larger size (MSNs). Because of their very large pore volume, these MSNs could also serve as a cargo for functional molecules (i.e. to trigger reactions from the islet cells). The present study provides the first comprehensive and quantitative MRI signal and contrast enhancement study performed on paramagnetic islets scanned for relatively long periods of time (weeks). The retention of Gd in the immune-protective capsule was demonstrated over a period of several months. Similar results were obtained when the alginate concentration was increased from 2% to 5% when generating the beads (data not shown). We previously observed mean alginate gel pore sizes of ~2 nm for 5% alginate beads and ~5 nm for 1.5% alginate beads produced by emulsification and internal gelation.[35] The long-term retention of the 166 ± 22 nm Gd-MSNs in the alginate gel network is therefore consistent with the expected alginate gel pore size distribution. While bead swelling may occur in vivo, a significant change would be required before the alginate pore dimensions reach the Gd-MSN size. In previous rodent studies, we did not observe any evidence of changes in bead size distribution 20 days after implantation, suggesting that the Gd-MSNs would also be retained in vivo.[35]

To determine the potential effects of Gd-MSNs on beta cells, MIN6 cells were used as a preliminary model to study Gd-MSN cytotoxicity. As shown in Figure 5, the MIN6 cells co-encapsulated with Gd-MSNs displayed a 2 day lag time that was not observed in the absence of Gd-MSNs. It is unlikely that the calculated lag time was due to cell death: no significant differences in cell density or viability were observed 24 h after encapsulation (Figure 6). The lag time could also simply be due to the confounding effect of the total processing time. Due to experimental limitations, the MIN6 cells co-encapsulated with Gd-MSNs were stored in medium at room temperature in equilibrium with air on average 3 hours longer prior to encapsulation than MIN6 cells encapsulated without Gd-MSNs. The resulting pH increase or time in suspension may have led to a lag in cell expansion after encapsulation.

Although the processing time or the presence of co-encapsulated Gd-MSNs was associated with an increased lag time, the co-encapsulated Gd-MSNs did not affect MIN6 cell cell cluster size

(Figure 6) or growth rate (Figure 7) over 2 weeks of culture. The similar cell viability and cell cluster morphology observed after 14 days suggest that the Gd-MSN effects – if any – subside after the initial lag period. The reduced MIN6 cell cluster density but similar cell cluster size with or without Gd-MSNs suggests that the lag time observed in Figure 7 was due to initial cell losses, and not to a reduction in cell growth rate or cell adaptation to the Gd-MSNs. These initial cell losses may have occurred during the additional 3 hours of processing time of the MIN6 cells co-encapsulated with Gd-MSNs, but initial Gd-MSN cytotoxicity followed by recovery cannot be ruled out. Future work will aim to determine the cause and minimize initial cell losses, for example by minimizing the time MIN6 cells are stored in suspension prior to encapsulation. Necrotic cores were observed in >50 µm diameter cell clusters obtained after 2 weeks of immobilized culture both with and without Gd-MSNs, as expected from oxygen mass transfer models and previous observations.[34] The Gd-MSNs also did not significantly affect *Ins1*, *Ins2*, *Pdx1* and *NKX6-1* gene expression. The encapsulation process and the Gd-MSNs both slightly but significantly increased the expression of *Glut*2 over the period of 2 weeks. Previous work has shown that *Glut2* expression decreases in glucose unresponsive islets[60]. In MIN6 cells, *Glut2* overexpression did not correlate with glucose responsiveness of cells[61]. The relationship between Gd-MSN exposure and increased *Glut2* expression by MIN6 cells should be further investigated, but is unlikely to have a negative impact on beta cell function.

Previous work has demonstrated that similar gadolinium-labeled MSNs were biocompatible.[62] Due to the encapsulation process, the Gd-MSNs are sequestered in the alginate. Therefore, the possibility of Gd-MSNs uptake by cells, and the related cytotoxicity risks, appear to be minimal. Contrary to MIN6 cells, adult mouse[63] and human[64] islets display very low replication rates, and are hence not expected to migrate through the beads or significantly disrupt the hydrogel that sequesters the Gd-MSNs. Furthermore, islets are cell clusters: the ratio of cells in contact with the Gd-MSNs and encapsulation material would be less significant than for the dispersed MIN6 cells seeded here. Nevertheless, an effect of the Gd-MSNs on MIN6 cell lag time and/or stress may have caused the observed lag time and change in *Glut2* expression. Future work will investigate the fate of the Gd-MSNs in the alginate network, the internalisation of Gd-MSNs by beta cells, as well as potential effects of the the Gd-MSNs on cell apoptosis, stress, metabolism and gene expression.

The co-encapsulation of paramagnetic particles and beta cells represents a significant advance towards monitoring encapsulated islets or other encapsulated therapeutics in vivo. The Gd-MSNs have the capacity for drug loading and potentially controlled drug delivery while allowing in vivo tracking of the process. The Gd-MSNs could also be used to study the stability of microbeads transplanted in sites other than the peritoneal cavity. The capacity to monitor encapsulated islets using MRI constitutes an important step towards developing safe immunoprotected islet transplantation technologies.

CONCLUSION

The non-invasive monitoring of microencapsulated islets could improve our understanding of factors that limit encapsulated islet survival in vivo. This study describes a novel Gd-MSN co-immobilization approach to image encapsulated beta cells using MRI. The co-encapsulation of Gd-MSNs with MIN6 beta cells did not lead to significant changes in MIN6 viability or growth rate. Further studies are needed to determine whether Gd-MSNs can be internalised by co-encapsulated beta cells or affect islet function. This work is the first to quantify the MRI contrast enhancement of alginate beads using gadolinium-based nanoparticles, and to demonstrate the ability of alginate beads to sequester Gd-MSNs over the long term. In addition to successful MRI signal enhancement, these Gd-MSNs are non-toxic. These versatile constructs have the ability to deliver drugs and other molecules through their loading capabilities. In addition to enabling MRI tracking, the Gd-MSNs could therefore be used to locally deliver factors that enhance encapsulated islet survival or function. The Gd-MSNs could be incorporated into a number of existing encapsulation devices to aid in vivo monitoring and optimize graft performance in order to develop a safe and effective treatement for type 1 diabetes.

AUTHOR INFORMATION

Corresponding Authors

*Corinne A. Hoesli, Department of Chemical Engineering, McGill University, Montreal, Quebec, Canada, H3A 0C5. Phone: 1-515-398-4275. E-mail: corinne.hoesli@mcgill.ca

*Marc-André Fortin, Laboratoire de Biomatériaux pour l'Imagerie médicale, Axe Médecine Régénératrice, Centre de recherche du Centre hospitalier universitaire de Québec (CR-CHU de Québec), 10 rue de l'Espinay, Québec, QC G1L 3L5, Canada. E-mail : marc-andre.fortin@gmn.ulaval.ca

Author Contributions

The manuscript was written through contributions of all authors. All authors have given approval to the final version of the manuscript. ‡These authors contributed equally.

Funding Sources

This project was funded by a Concours de subvention aux projets collaboratifs 2014-2015 of the Centre Québécois sur les matériaux fonctionnels (CQMF, award number FRQNT/Université Laval 144482). This work was also supported by the Quebec Network for cell and tissue therapies –ThéCell (a thematic network funded by the Fonds de recherche du Québec–Santé, award dossier number 20066).

ACKNOWLEDGEMENTS

The authors would like to acknowledge the valuable contributions from Dr. Diane Djoumessi (TEM images), Mrs Meryem Bouchoucha (TGA and nitrogen physisorption analysis), Dr. Pascale Chevallier (DLS measurements and relaxometric analysis) as well as Dr. Jean Lagueux (MRI studies). We also thank Dr. Marta Szabat and Dr. James D. Johnson at UBC for sharing the MIN6 cell line. MRI acquisitions were performed at CR-CHU de Quebec's Small-Animal Imaging Platform. We thank the Montréal Diabetes Research Center for their support of regional diabetes research and networking activities.

DESCRIPTION OF THE SUPPORTING INFORMATION

The following files are available free of charge.

Supplementary methods and results: characterization of the Gd-MSNs and list of PCR primers (contains Figure S1, Figure S2, Table S1, Table S2, Table S3). (PDF).

ABBREVIATIONS

ActB, beta-actin; APTES (3-aminopropyl)triethoxysilane; DLS, dynamic light scattering; DMEM, Dulbecco's Modified Eagle's Medium; DMSO, dimethyl sulfoxide; DTPA, diethylene triamine pentaacetic acid; *Gapdh*, glyceraldehyde 3-phosphate dehydrogenase; Gd-MSN, gadolinium-labeled mesoporous silica nanoparticles; *Glut2*, glucose transporter 2; HEPES, (4-(2-hydroxy ethyl)-1-piperazineethanesulfonic acid); *Ins1*, mouse insulin I; *Ins2*, mouse insulin II; MIN6, mouse insulinoma 6, MSN, mesoporous silica nanoparticles; NAA, neutron activation analysis; *NKX6-1*, homeobox protein Nkx-6.1; pdx1, pancreas/duodenum homeobox protein 1; TEM, transmission electron microscopy; TEOS, tetraethylorthosilicate; TGA, thermal differential analysis; XRD, low-angle X-ray diffraction.

REFERENCES

1. Atkinson, M. A.; Eisenbarth, G. S.; Michels, A. W., Type 1 diabetes. *The Lancet 383* (9911), 69-82. DOI: http://dx.doi.org/10.1016/S0140-6736(13)60591-7.
2. CDC *Canadian Diabetes Association 2015 Pre-Budget Submission to the House of Common Standing Committee on Finance*; Canadian Diabetes Association: 2014; p 8.
3. Barton, F. B.; Rickels, M. R.; Alejandro, R.; Hering, B. J.; Wease, S.; Naziruddin, B.; Oberholzer, J.; Odorico, J. S.; Garfinkel, M. R.; Levy, M.; Pattou, F.; Berney, T.; Secchi, A.; Messinger, S.; Senior, P. A.; Maffi, P.; Posselt, A.; Stock, P. G.; Kaufman, D. B.; Luo, X. R.; Kandeel, F.; Cagliero, E.; Turgeon, N. A.; Witkowski, P.; Naji, A.; O'Connell, P. J.; Greenbaum, C.; Kudva, Y. C.; Brayman, K. L.; Aull, M. J.; Larsen, C.; Kay, T. W. H.; Fernandez, L. A.; Vantyghem, M. C.; Bellin, M.; Shapiro, A. M. J., Improvement in Outcomes of Clinical Islet Transplantation: 1999-2010. *Diabetes Care* **2012,** *35* (7), 1436-1445. DOI: 10.2337/dc12-0063.
4. Hirshberg, B.; Rother, K. I.; Digon, B. J.; Lee, J.; Gaglia, J. L.; Hines, K.; Read, E. J.; Chang, R.; Wood, B. J.; Harlan, D. M., Benefits and Risks of Solitary Islet Transplantation for Type 1 Diabetes Using Steroid-Sparing Immunosuppression. *The National Institutes of Health experience* **2003,** *26* (12), 3288-3295. DOI: 10.2337/diacare.26.12.3288.
5. Hering, B. J.; Clarke, W. R.; Bridges, N. D.; Eggerman, T. L.; Alejandro, R.; Bellin, M. D.; Chaloner, K.; Czarniecki, C. W.; Goldstein, J. S.; Hunsicker, L. G.; Kaufman, D. B.; Korsgren, O.; Larsen, C. P.; Luo, X. R.; Markmann, J. F.; Naji, A.; Oberholzer, J.; Posselt, A. M.; Rickels, M. R.; Ricordi, C.; Robien, M. A.; Senior, P. A.; Shapiro, A. M. J.; Stock, P. G.; Turgeon, N. A.; Con, C. I. T., Phase 3 Trial of Transplantation of Human Islets in Type 1 Diabetes Complicated by Severe Hypoglycemia. *Diabetes Care* **2016,** *39* (7), 1230-1240. DOI: 10.2337/dc15-1988.
6. Low, G.; Hussein, N.; Owen, R. J.; Toso, C.; Patel, V. H.; Bhargava, R.; Shapiro, A. J., Role of Imaging in Clinical Islet Transplantation 1. *Radiographics* **2010,** *30* (2), 353-366.

7. Desai, N. M.; Goss, J. A.; Deng, S.; Wolf, B. A.; Markmann, E.; Palanjian, M.; Shock, A. P.; Feliciano, S.; Brunicardi, F. C.; Barker, C. F., Elevated portal vein drug levels of sirolimus and tacrolimus in islet transplant recipients: local immunosuppression or islet toxicity? 1. *Transplantation* **2003,** *76* (11), 1623-1625.
8. Zhang, N.; Su, D.; Qu, S.; Tse, T.; Bottino, R.; Balamurugan, A. N.; Xu, J.; Bromberg, J. S.; Dong, H. H., Sirolimus Is Associated With Reduced Islet Engraftment and Impaired β-Cell Function. *Diabetes* **2006,** *55* (9), 2429-2436. DOI: 10.2337/db06-0173.
9. Lim, F.; Sun, A., Microencapsulated islets as bioartificial endocrine pancreas. *Science* **1980,** *210* (4472), 908-910. DOI: 10.1126/science.6776628.
10. Calafiore, R.; Basta, G.; Luca, G.; Calvitti, M.; Calabrese, G.; Racanicchi, L.; Macchiarulo, G.; Mancuso, F.; Guido, L.; Brunetti, P., Grafts of microencapsulated pancreatic islet cells for the therapy of diabetes mellitus in non-immunosuppressed animals. *Biotechnol Appl Bioc* **2004,** *39*, 159-164. DOI: Doi 10.1042/Ba20030151.
11. Duvivier-Kali, V. F.; Omer, A.; Parent, R. J.; O'Neil, J. J.; Weir, G. C., Complete protection of islets against allorejection and autoimmunity by a simple barium-alginate membrane. *Diabetes* **2001,** *50* (8), 1698-1705. DOI: DOI 10.2337/diabetes.50.8.1698.
12. Soonshiong, P.; Feldman, E.; Nelson, R.; Komtebedde, J.; Smidsrod, O.; Skjakbraek, G.; Espevik, T.; Heintz, R.; Lee, M., Successful Reversal of Spontaneous Diabetes in Dogs by Intraperitoneal Microencapsulated Islets. *Transplantation* **1992,** *54* (5), 769-774. DOI: Doi 10.1097/00007890-199211000-00001.
13. Strand, B. L.; Coron, A. E.; Skjak-Braek, G., Current and Future Perspectives on Alginate Encapsulated Pancreatic Islet. *Stem Cells Transl Med* **2017**. DOI: 10.1002/sctm.16-0116.
14. Souza, Y. E. D. M. d.; Chaib, E.; Lacerda, P. G. d.; Crescenzi, A.; Bernal-Filho, A.; D'Albuquerque, L. A. C., Islet transplantation in rodents: do encapsulated islets really work? *Arquivos de Gastroenterologia* **2011,** *48*, 146-152.
15. Korbutt, G. S.; Mallett, A. G.; Ao, Z.; Flashner, M.; Rajotte, R. V., Improved survival of microencapsulated islets during in vitro culture and enhanced metabolic function following transplantation. *Diabetologia* **2004,** *47* (10), 1810-1818. DOI: 10.1007/s00125-004-1531-3.
16. Scharp, D. W.; Marchetti, P., Encapsulated islets for diabetes therapy: history, current progress, and critical issues requiring solution. *Adv Drug Deliv Rev* **2014,** *67-68*, 35-73. DOI: 10.1016/j.addr.2013.07.018.
17. Arifin, D. R.; Bulte, J. W., Imaging of pancreatic islet cells. *Diabetes/metabolism research and reviews* **2011,** *27* (8), 761-766.
18. Barnett, B. P.; Arepally, A.; Karmarkar, P. V.; Qian, D.; Gilson, W. D.; Walczak, P.; Howland, V.; Lawler, L.; Lauzon, C.; Stuber, M.; Kraitchman, D. L.; Bulte, J. W. M., Magnetic resonance-guided, real-time targeted delivery and imaging of magnetocapsules immunoprotecting pancreatic islet cells. *Nat Med* **2007,** *13* (8), 986-991. DOI: http://www.nature.com/nm/journal/v13/n8/suppinfo/nm1581_S1.html.
19. Tai, J. H.; Foster, P.; Rosales, A.; Feng, B.; Hasilo, C.; Martinez, V.; Ramadan, S.; Snir, J.; Melling, C. W. J.; Dhanvantari, S.; Rutt, B.; White, D. J. G., Imaging Islets Labeled With Magnetic Nanoparticles at 1.5 Tesla. *Diabetes* **2006,** *55* (11), 2931-2938. DOI: 10.2337/db06-0393.
20. Evgenov, N. V.; Medarova, Z.; Pratt, J.; Pantazopoulos, P.; Leyting, S.; Bonner-Weir, S.; Moore, A., In Vivo Imaging of Immune Rejection in Transplanted Pancreatic Islets. *Diabetes* **2006,** *55* (9), 2419-2428. DOI: 10.2337/db06-0484.

21. Evgenov, N. V.; Medarova, Z.; Dai, G.; Bonner-Weir, S.; Moore, A., In vivo imaging of islet transplantation. *Nat Med* **2006,** *12* (1), 144-148. DOI: http://www.nature.com/nm/journal/v12/n1/suppinfo/nm1316_S1.html.
22. Jirák, D.; Kríz, J.; Herynek, V.; Andersson, B.; Girman, P.; Burian, M.; Saudek, F.; Hájek, M., MRI of transplanted pancreatic islets. *Magn.Reson.Med.* **2004,** *52* (6), 1228-1233. DOI: 10.1002/mrm.20282.
23. Heyn, C.; Ronald, J. A.; Mackenzie, L. T.; MacDonald, I. C.; Chambers, A. F.; Rutt, B. K.; Foster, P. J., In vivo magnetic resonance imaging of single cells in mouse brain with optical validation. *Magn Reson Med* **2006,** *55* (1), 23-9. DOI: 10.1002/mrm.20747.
24. Evgenov, N. V.; Medarova, Z.; Pratt, J.; Pantazopoulos, P.; Leyting, S.; Bonner-Weir, S.; Moore, A., In vivo imaging of immune rejection in transplanted pancreatic islets. *Diabetes* **2006,** *55* (9), 2419-28. DOI: 10.2337/db06-0484.
25. Evgenov, N. V.; Medarova, Z.; Dai, G.; Bonner-Weir, S.; Moore, A., In vivo imaging of islet transplantation. *Nat Med* **2006,** *12* (1), 144-8. DOI: 10.1038/nm1316.
26. Caravan, P., Strategies for increasing the sensitivity of gadolinium based MRI contrast agents. *Chem Soc Rev* **2006,** *35* (6), 512-23. DOI: 10.1039/b510982p.
27. Biancone, L.; Crich, S. G.; Cantaluppi, V.; Romanazzi, G. M.; Russo, S.; Scalabrino, E.; Esposito, G.; Figliolini, F.; Beltramo, S.; Perin, P. C., Magnetic resonance imaging of gadolinium-labeled pancreatic islets for experimental transplantation. *NMR in biomedicine* **2007,** *20* (1), 40-48.
28. Menakbi, C.; Quignard, F.; Mineva, T., Complexation of Trivalent Metal Cations to Mannuronate Type Alginate Models from a Density Functional Study. *J Phys Chem B* **2016,** *120* (15), 3615-23. DOI: 10.1021/acs.jpcb.6b00472.
29. Bouchoucha, M.; C.-Gaudreault, R.; Fortin, M.-A.; Kleitz, F., Mesoporous Silica Nanoparticles: Selective Surface Functionalization for Optimal Relaxometric and Drug Loading Performances. *Advanced Functional Materials* **2014,** *24* (37), 5911-5923. DOI: 10.1002/adfm.201400524.
30. Bouchoucha, M.; Cote, M. F.; C-Gaudreault, R.; Fortin, M. A.; Kleitz, F., Size-Controlled Functionalized Mesoporous Silica Nanoparticles for Tunable Drug Release and Enhanced Anti-Tumoral Activity. *Chem. Mat.* **2016,** *28* (12), 4243-4258. DOI: 10.1021/acs.chemmater.6b00877.
31. Laprise-Pelletier, M.; Bouchoucha, M.; Lagueux, J.; Chevallier, P.; Lecomte, R.; Gossuin, Y.; Kleitz, F.; Fortin, M. A., Metal chelate grafting at the surface of mesoporous silica nanoparticles (MSNs): physico-chemical and biomedical imaging assessment. *J Mater Chem B* **2015,** *3* (5), 748-758. DOI: 10.1039/c4tb01423e.
32. Singh, N.; Karambelkar, A.; Gu, L.; Lin, K.; Miller, J. S.; Chen, C. S.; Sailor, M. J.; Bhatia, S. N., Bioresponsive mesoporous silica nanoparticles for triggered drug release. *Journal of the American Chemical Society* **2011,** *133* (49), 19582-19585.
33. Bowers, D. T.; Botchwey, E. A.; Brayman, K. L., Advances in Local Drug Release and Scaffolding Design to Enhance Cell Therapy for Diabetes. *Tissue Eng Part B Rev* **2015,** *21* (6), 491-503. DOI: 10.1089/ten.TEB.2015.0275.
34. Hoesli, C. A.; Raghuram, K.; Kiang, R. L. J.; Mocinecová, D.; Hu, X.; Johnson, J. D.; Lacík, I.; Kieffer, T. J.; Piret, J. M., Pancreatic cell immobilization in alginate beads produced by emulsion and internal gelation. *Biotechnology and Bioengineering* **2011,** *108* (2), 424-434. DOI: 10.1002/bit.22959.

35. Hoesli, C. A.; Kiang, R. L. J.; Mocinecová, D.; Speck, M.; Mošková, D. J.; Donald-Hague, C.; Lacík, I.; Kieffer, T. J.; Piret, J. M., Reversal of diabetes by βTC3 cells encapsulated in alginate beads generated by emulsion and internal gelation. *Journal of Biomedical Materials Research Part B: Applied Biomaterials* **2012,** *100B* (4), 1017-1028. DOI: 10.1002/jbm.b.32667.

36. Ishihara, H.; Asano, T.; Tsukuda, K.; Katagiri, H.; Inukai, K.; Anai, M.; Kikuchi, M.; Yazaki, Y.; Miyazaki, J.-I.; Oka, Y., Pancreatic beta cell line MIN6 exhibits characteristics of glucose metabolism and glucose-stimulated insulin secretion similar to those of normal islets. *Diabetologia* **1993,** *36* (11), 1139-1145. DOI: 10.1007/bf00401058.

37. Silencieux, F.; Bouchoucha, M.; Mercier, O.; Turgeon, S.; Chevallier, P.; Kleitz, F.; Fortin, M. A., Mesoporous Silica Nanoparticles under Sintering Conditions: A Quantitative Study. *Langmuir* **2015,** *31* (47), 13011-13021. DOI: 10.1021/acs.langmuir.5b02961.

38. Schneider, C. A.; Rasband, W. S.; Eliceiri, K. W., NIH Image to ImageJ: 25 years of image analysis. *Nat Methods* **2012,** *9* (7), 671-5.

39. Fröhlich, E.; Bonstingl, G.; Höfler, A.; Meindl, C.; Leitinger, G.; Pieber, T. R.; Roblegg, E., Comparison of two in vitro systems to assess cellular effects of nanoparticles-containing aerosols. *Toxicology in Vitro* **2013,** *27* (1), 409-417. DOI: http://dx.doi.org/10.1016/j.tiv.2012.08.008.

40. Naccache, R.; Chevallier, P.; Lagueux, J.; Gossuin, Y.; Laurent, S.; Vander Elst, L.; Chilian, C.; Capobianco, J. A.; Fortin, M. A., Imaging: high relaxivities and strong vascular signal enhancement for NaGdF4 nanoparticles designed for dual MR/optical imaging (Adv. Healthcare Mater. 11/2013). *Adv Healthc Mater* **2013,** *2* (11), 1477. DOI: 10.1002/adhm.201370057.

41. Hoesli, C. A.; Kiang, R. L. J.; Raghuram, K.; Pedroza, R. G.; Markwick, K. E.; Colantuoni, A. M. R.; Piret, J. M., Mammalian Cell Encapsulation in Alginate Beads Using a Simple Stirred Vessel. *J Vis Exp* **2017,** (124). DOI: 10.3791/55280.

42. Carpenter, A. E.; Jones, T. R.; Lamprecht, M. R.; Clarke, C.; Kang, I. H.; Friman, O.; Guertin, D. A.; Chang, J. H.; Lindquist, R. A.; Moffat, J.; Golland, P.; Sabatini, D. M., CellProfiler: image analysis software for identifying and quantifying cell phenotypes. *Genome Biol* **2006,** *7* (10), R100. DOI: 10.1186/gb-2006-7-10-r100.

43. Kim, T. W.; Chung, P. W.; Lin, V. S. Y., Facile Synthesis of Monodisperse Spherical MCM-48 Mesoporous Silica Nanoparticles with Controlled Particle Size. *Chem. Mat.* **2010,** *22* (17), 5093-5104. DOI: 10.1021/cm1017344.

44. Guillet-Nicolas, R.; Bridot, J. L.; Seo, Y.; Fortin, M. A.; Kleitz, F., Enhanced Relaxometric Properties of MRI "Positive" Contrast Agents Confined in Three-Dimensional Cubic Mesoporous Silica Nanoparticles. *Advanced Functional Materials* **2011,** *21* (24), 4653-4662. DOI: 10.1002/adfm.201101766.

45. Schmidt, R.; Stocker, M.; Ellestad, O. H., Characterisation of a cubic mesoporous MCM-48 compared to a hexagonal MCM-41. *Stud Surf Sci Catal* **1995,** *97*, 149-156.

46. Fernandez, S. A.; Dussault, M.-A.; Bégin-Drolet, A.; Ruel, J.; Leask, R.; Hoesli, C. A., Towards the fabrication of a 3D printed vascularized islet transplantation device for the treatment of type 1 diabetes. *Front. Bioeng. Biotechnol.* **2016,** *4*. DOI: 10.3389/conf.fbioe.2016.01.01021.

47. Caravan, P.; Farrar, C. T.; Frullano, L.; Uppal, R., Influence of molecular parameters and increasing magnetic field strength on relaxivity of gadolinium- and manganese-based T1 contrast agents. *Contrast media & molecular imaging* **2009,** *4* (2), 89-100. DOI: 10.1002/cmmi.267.

48. Hoesli, C. Bioprocess development for the cell-based treatment of diabetes. University of British Columbia, https://open.library.ubc.ca/cIRcle/collections/24/items/1.0058832, 2010.
49. Giuliani, M.; Moritz, W.; Bodmer, E.; Dindo, D.; Kugelmeier, P.; Lehmann, R.; Gassmann, M.; Groscurth, P.; Weber, M., Central Necrosis in Isolated Hypoxic Human Pancreatic Islets: Evidence for Postisolation Ischemia. *Cell Transplantation* **2005,** *14* (1), 67-76. DOI: 10.3727/000000005783983287.
50. Andralojc, K.; Srinivas, M.; Brom, M.; Joosten, L.; de Vries, I. J. M.; Eizirik, D. L.; Boerman, O. C.; Meda, P.; Gotthardt, M., Obstacles on the way to the clinical visualisation of beta cells: looking for the Aeneas of molecular imaging to navigate between Scylla and Charybdis. *Diabetologia* **2012,** *55* (5), 1247-1257. DOI: 10.1007/s00125-012-2491-7.
51. Arifin, D. R.; Bulte, J. W. M., Imaging of pancreatic islet cells. *Diabetes-Metab. Res. Rev.* **2011,** *27* (8), 761-766. DOI: 10.1002/dmrr.1248.
52. Borot, S.; Crowe, L. A.; Toso, C.; Vallee, J. P.; Berney, T., Noninvasive Imaging Techniques in Islet Transplantation. *Curr. Diabetes Rep.* **2011,** *11* (5), 375-383. DOI: 10.1007/s11892-011-0215-x.
53. Barnett, B. P.; Arepally, A.; Stuber, M.; Arifin, D. R.; Kraitchman, D. L.; Bulte, J. W. M., Synthesis of magnetic resonance-, X-ray- and ultrasound-visible alginate microcapsules for immunoisolation and noninvasive imaging of cellular therapeutics. *Nat. Protoc.* **2011,** *6* (8), 1142-1151. DOI: 10.1038/nprot.2011.352.
54. Kim, J.; Arifin, D. R.; Muja, N.; Kim, T.; Gilad, A. A.; Kim, H.; Arepally, A.; Hyeon, T.; Bulte, J. W. M., Multifunctional Capsule-in-Capsules for Immunoprotection and Trimodal Imaging. *Angewandte Chemie International Edition* **2011,** *50* (10), 2317-2321. DOI: 10.1002/anie.201007494.
55. Sosnovik, D. E.; Nahrendorf, M.; Weissleder, R., Magnetic nanoparticles for MR imaging: agents, techniques and cardiovascular applications. *Basic Res. Cardiol.* **2008,** *103* (2), 122-130. DOI: 10.1007/s00395-008-0710-7.
56. Biancone, L.; Crich, S. G.; Cantaluppi, V.; Romanazzi, G. M.; Russo, S.; Scalabrino, E.; Esposito, G.; Figliolini, F.; Beltramo, S.; Perin, P. C.; Segoloni, G. P.; Aime, S.; Camussi, G., Magnetic resonance imaging of gadolinium-labeled pancreatic islets for experimental transplantation. *NMR in Biomedicine* **2007,** *20* (1), 40-48. DOI: 10.1002/nbm.1088.
57. Cabella, C.; Crich, S. G.; Corpillo, D.; Barge, A.; Ghirelli, C.; Bruno, E.; Lorusso, V.; Uggeri, F.; Aime, S., Cellular labeling with Gd(III) chelates: only high thermodynamic stabilities prevent the cells acting as 'sponges' of Gd3+ ions. *Contrast Media Mol Imaging* **2006,** *1* (1), 23-9. DOI: 10.1002/cmmi.88.
58. Arifin, D. R.; Long, C. M.; Gilad, A. A.; Alric, C.; Roux, S.; Tillement, O.; Link, T. W.; Arepally, A.; Bulte, J. W. M., Trimodal Gadolinium-Gold Microcapsules Containing Pancreatic Islet Cells Restore Normoglycemia in Diabetic Mice and Can Be Tracked by Using US, CT, and Positive-Contrast MR Imaging. *Radiology* **2011,** *260* (3), 790-798. DOI: 10.1148/radiol.11101608.
59. Waeber, G.; Thompson, N.; Nicod, P.; Bonny, C., Transcriptional activation of the GLUT2 gene by the IPF-1/STF-1/IDX-1 homeobox factor. *Molecular Endocrinology* **1996,** *10* (11), 1327-1334. DOI: doi:10.1210/mend.10.11.8923459.
60. Guillam, M.-T.; Hümmler, E.; Schaerer, E.; Wu, J.-Y.; Birnbaum, M. J.; Beermann, F.; Schmidt, A.; Dériaz, N.; Thorens, B., Early diabetes and abnormal postnatal pancreatic islet development in mice lacking Glut-2. *Nature genetics* **1997,** *17* (3), 327-330.

61. Ishihara, H.; Asano, T.; Tsukuda, K.; Katagiri, H.; Inukai, K.; Anai, M.; Yazaki, Y.; Miyazaki, J.; Kikuchi, M.; Oka, Y., Human GLUT-2 overexpression does not affect glucose-stimulated insulin secretion in MIN6 cells. *American Journal of Physiology - Endocrinology and Metabolism* **1995,** *269* (5), E897-E902.
62. Huang, C.-H.; Tsourkas, A., Gd-based macromolecules and nanoparticles as magnetic resonance contrast agents for molecular imaging. *Current topics in medicinal chemistry* **2013,** *13* (4), 411-421.
63. Dor, Y.; Brown, J.; Martinez, O. I.; Melton, D. A., Adult pancreatic [beta]-cells are formed by self-duplication rather than stem-cell differentiation. *Nature* **2004,** *429* (6987), 41-46.
64. Cnop, M.; Hughes, S. J.; Igoillo-Esteve, M.; Hoppa, M. B.; Sayyed, F.; van de Laar, L.; Gunter, J. H.; de Koning, E. J.; Walls, G. V.; Gray, D. W.; Johnson, P. R.; Hansen, B. C.; Morris, J. F.; Pipeleers-Marichal, M.; Cnop, I.; Clark, A., The long lifespan and low turnover of human islet beta cells estimated by mathematical modelling of lipofuscin accumulation. *Diabetologia* **2010,** *53* (2), 321-30. DOI: 10.1007/s00125-009-1562-x.

TABLE OF CONTENT GRAPHIC

Title: Magnetic resonance imaging of alginate beads containing pancreatic beta cells and paramagnetic nanoparticles

Author names: Sary Sarkis, Fanny Silencieux, Karen E. Markwick, Marc-André Fortin, Corinne A. Hoesli